Pergamon

Int. J. Heat Mass Transfer. Vol. 38, No. 15, pp. 2715–2722, 1995

0017–9310/95 $9.50+0.00

0017–9310(95)00083–6

Flow dynamics and heat transfer of a condensate film on a vertical wall—II. Flow dynamics and heat transfer

ERICH STUHLTRÄGER
Balzers Ltd, FL-9496 Balzers, Liechtenstein

and

AKIO MIYARA† and HARUO UEHARA
Saga University, 1 Honjo-machi Saga-shi, Saga 840, Japan

(*Received* 26 *October* 1994 *and in final form* 16 *February* 1995)

Abstract—The effects of waves occurring on a falling condensate film on heat transfer have been studied by direct computer simulation. The time-dependent Navier–Stokes and energy equations, as well as the Poisson equation for pressure, have been solved for a condensate film of R11 from the leading edge to 0.6 m with finite difference schemes and non-periodic boundary conditions The waves, which have amplitude of the order of the film substrate, were observed in the region of $200 < Re < 455$, and the heat transfer coefficient is increased by about 60%, while it is identical with the Nusselt theory at $Re < 120$. In this simulation range the enhancement of the heat transfer is attributed to the decreasing time averaged film thickness due to waves, and the disturbance effects of the waves are small.

1. INTRODUCTION

Many experimental data and theoretical studies have been presented on the heat transfer of a vertically falling condensate film. Although most experimental data show higher values than the Nusselt theory for a laminar condensate film [1] due to waves on the film surface, very few studies have considered the relation between the heat transfer and flow dynamics.

Experimentally obtained average heat transfer coefficients of the condensing water vapor [2–4] have the same values obtained from the Nusselt theory in the region of $Re < 30$, and the heat transfer coefficients become higher than those given by the Nusselt theory for $Re > 30$. The experimental data are about 50% higher at $Re = 1000$. Selin [5] conducted experiments with pure vapors of butanol and propanol in the region of $400 < Re < 1000$; his data for heat transfer coefficients are also 50% higher than the predictions of the Nusselt theory. Struve [6] used a measurement cell size 0.05 m in his experiment on an evaporating falling film of R11 and obtained local heat transfer coefficients which are already about 20% higher than the one of the Nusselt solution at $Re > 50$. Chun and Seban [7] measured the local heat transfer coefficient of evaporating water film on a 0.305 m cell with a 0.305 m unheated entry length. The data indicate about 60% higher heat transfer coefficient at $300 < Re < 1000$ than the Nusselt theory. Uehara and Kinoshita [8] made experiments on wavy and turbulent condensate films of R11, R113 and R123 on a vertical surface 3 m in length, and they proposed correlations for the local heat transfer coefficient.

Hirshburg and Florschuetz [9, 10] established a linearized theory for a falling film without condensation in a coordinate system moving with the waves by assuming periodicity and a parabolic profile. Two asymptotic wavy flow states were found, namely the so-called sinusoidal wave and intermediate wave solution. The sinusoidal wave shape has a distortion factor, which is defined as the ratio of the actual frequency to the most unstable frequency, of $f^+ = 1$; for the intermediate wave f^+ varies from 1 to 0.35. The theory provides the length, celerity and amplitude of the wave as well as the Nusselt number of different wave shapes. The calculated value was consistent with experimental data.

The purpose of this unsteady computer simulation of the condensate falling film is to investigate the relation between the film flow dynamics and the heat transfer coefficient. The unsteady basic equations, namely the Navier–Stokes equation, the energy equation and the Poisson equation for pressure, and the computational method have been explained and the flow dynamics of the falling condensate film were discussed in part I [11]. In the present study temperature fields have been solved in addition to velocity fields and the heat transfer coefficient of a wavy condensate

†Author to whom correspondence should be addressed.

NOMENCLATURE

- Fr_0 Froude number at the outflow location, $u_0^2/(g\delta_0)$
- G mass flow rate of film per unit film width [kg m^{-1} s^{-1}]
- h heat transfer coefficient [W m^{-2} K^{-1}]
- i mesh point index number in the x-direction
- I biggest mesh point index number in the x-direction at the outflow
- j mesh point index number in the y-direction
- J biggest mesh point index number in the y-direction, beyond the surface
- J_s index number of the surface point
- k thermal conductivity of liquid [W m^{-1} K^{-1}]
- L latent heat [J]
- $\dot{m}$ condensing rate per unit area [kg m^{-2} s^{-1}]
- Nu condensation number, $h(v^2/g)^{1/3}/k$
- p pressure
- Pr Prandtl number
- Re film Reynolds number, $4G/\mu$
- Re_0 Reynolds number at the outflow location, $u_0\delta_0/v$
- t time
- T temperature
- u velocity parallel to the condensation plate
- v velocity perpendicular to the condensation plate
- We_0 Weber number, $\rho_0 u_0^2\delta_0/\sigma$
- x coordinate parallel to the condensation plate
- y coordinate perpendicular to the condensation plate.

Greek symbols

- δ film thickness
- μ dynamic viscosity [kg s m^{-1}]
- v kinetic viscosity [m^2 s^{-1}]
- ρ density of the liquid [kg m^{-3}]
- σ surface tension [N m^{-1}].

Subscripts

- l liquid
- 0 standard value at the outflow location
- s surface
- v vapor
- w wall
- x local value at the position x.

Superscripts

- * parameter having its dimension
- ‾ time-averaged value.

film has been obtained. The important points of this computer simulation are as follows:

(1) the simulation was performed for the condensate film in the region from the leading edge of condensation to the occurrence of big merging waves;

(2) the unsteady basic equations were solved by time-step advance with a finite difference method without a turbulence model, which allows the simulation of the transition from laminar to turbulent flow;

(3) no periodic and as few as necessary fixed boundary conditions were employed.

2. FUNDAMENTAL EQUATIONS

In the previous study [11] the two-dimensional time-dependent Navier–Stokes equations, the Poisson equation for the pressure and the energy equation without the convection terms were solved by finite difference schemes. In the present study the two-dimensional time-dependent energy equation is used without neglecting the convection terms. Except for the energy equation, the same equations are used in this simulation. The basic equations are non-dimensionalized with the surface velocity u_0 and film thickness δ_0 at the outflow location of the calculation field obtained from the Nusselt theory, the saturation temperature T_s and the wall temperature T_w. The coordinate and velocities parallel and perpendicular to the wall are $x = x^*/\delta_0$, $y = y^*/\delta_0$, $u = u^*/u_0$ and $v = v^*/u_0$, respectively. The pressure is $p = p^*/(\rho_0 u_0^2)$ and the time $t = t^*/(\delta_0/u_0)$. The temperature is $T = (T^* - T_w)/(T_s - T_w)$.

The continuity equation and the Navier–Stokes equations are

$$\frac{\partial u}{\partial x} + \frac{\partial v}{\partial y} = 0 \tag{1}$$

$$\frac{\partial u}{\partial t} + u\frac{\partial u}{\partial x} + v\frac{\partial u}{\partial y} = -\frac{\partial p}{\partial x} + \frac{1}{Re_0}\left(\frac{\partial^2 u}{\partial x^2} + \frac{\partial^2 u}{\partial y^2}\right) + \frac{1}{Fr_0} \tag{2}$$

$$\frac{\partial v}{\partial t} + u\frac{\partial v}{\partial x} + v\frac{\partial v}{\partial y} = -\frac{\partial p}{\partial y} + \frac{1}{Re_0}\left(\frac{\partial^2 v}{\partial x^2} + \frac{\partial^2 v}{\partial y^2}\right) \tag{3}$$

where Re_0 is the Reynolds number at the outflow position obtained from the Nusselt theory and Fr_0 is the Froude number. The Poisson equation to solve the pressure field is derived from the Navier–Stokes equations (2), (3) as follows:

$$\nabla^2 p = -\frac{\partial D}{\partial t} - \left(\frac{\partial u}{\partial y}\right)^2 - \left(\frac{\partial v}{\partial y}\right)^2 - 2\frac{\partial v}{\partial x}\frac{\partial u}{\partial y} + \frac{1}{Re_0}\left(\frac{\partial^2 D}{\partial x^2} + \frac{\partial^2 D}{\partial y^2}\right) \quad (4)$$

$$D = \frac{\partial u}{\partial x} + \frac{\partial v}{\partial y}. \quad (5)$$

The energy equation is

$$\frac{\partial T}{\partial t} + u\frac{\partial T}{\partial x} + v\frac{\partial T}{\partial y} = \frac{1}{Re_0 Pr}\left(\frac{\partial^2 T}{\partial x^2} + \frac{\partial^2 T}{\partial y^2}\right). \quad (6)$$

In this calculation fixed boundary conditions are given only for indispensable values, which are velocities in the x and y directions on the plate surface, temperatures on the plate surface and the condensate film surface, and velocities, film thickness and temperature at a small part of the leading edge of the plate, values of which are given from the Nusselt theory.

Boundary conditions for the velocities and temperature on the plate surface ($y = 0$) and the film surface ($y = \delta$) are as follows.

$$y = 0: u = 0 \quad v = 0 \quad T = 0 \quad (7)$$

$$y = \delta: u = u_s \quad v = v_s \quad \frac{\partial u}{\partial y} = 0 \quad T = 1 \quad (8)$$

where u_s and v_s, which are x and y component velocities at the film surface, are calculated using the Navier–Stokes equations. With the assumption that the wavelength is much bigger than the film thickness, the pressure at the film surface p_s is calculated with the following equation:

$$(p_s - p_v) + \frac{1}{We_0}\frac{\partial^2 \delta}{\partial x^2} + \frac{2}{Re_0}\frac{\partial u_s}{\partial x} = 0 \quad (9)$$

where p_v is vapor pressure. The kinematic boundary condition for the falling film surface with condensation is

$$\frac{\partial \delta}{\partial t} = v_s - u_s\frac{\partial \delta}{\partial x} + \frac{\dot{m}}{\rho u_0} \quad (10)$$

where δ is film thickness and $\dot{m}$ is condensing rate per unit area.

For the boundary condition at the outflow, the method of Shapiro and O'Brien [13] was chosen. In this method a linear extrapolation is used in order to follow the Lagrange trajectory of a particle and to get outflow boundary values.

3. NUMERICAL SIMULATION METHOD

The computer simulation was performed for a condensate film of R11 on a vertical wall in the region from the leading edge to 0.6 m. The calculations were carried out in a rectangular region on the staggered grid points. The grid for the velocity u was placed on the wall surface and the grid for the velocity v was put before and behind the wall surface.

The timestep advance of the Navier–Stokes equation and the energy equation was made with the Euler explicit scheme. For the convective term, the third order upwind scheme proposed by Kawamura and Kuwahara [12] was used. The central difference scheme was employed for all the other terms. Velocities of x and y components, film thickness and temperature of the first three rows of the staggered grid have to be given from the Nusselt theory because the third order upwind scheme requires two adjoining points to the center point in every direction. For the same reason, the third order upwind scheme cannot be applied at the nearest points to the surface $j = J$, the adjacent point $j = J-1$, and the nearest points to the outflow boundary $i = I-1$. At the points $j = J-1$ and $i = I-1$, the donor cell method was applied instead of the third order upwind scheme. The velocity $u(i, J)$ was interpolated by a parabolic curve determined from the velocity on the surface $u_s(i)$ and the two other velocities $u(i, J-1)$ and $u(i, J-2)$. The velocity $v(i, J)$ was obtained from the continuity equation. The temperature $T(i, J)$ was calculated in the same way as $u(i, J)$. The values of the velocities and temperature at the wall surface are given as follows

$$u(i, 0) = 0 \quad (11)$$

$$u(i, -1) = -u(i, 1) \quad (12)$$

$$v(i, 0) = -v(i, 1) \quad (13)$$

$$T(i, 0) = 0 \quad (14)$$

$$T(i, -1) = -T(i, 1). \quad (15)$$

The Poisson equation for the pressure was solved using the Successive Over-Relaxation (SOR) method. Since the boundary conditions are complicated, an analytical calculation for the relaxation factor cannot be done. The relaxation factor was first calculated for Neumann boundary conditions and, by varying the factor in the real field slightly, the one with the fastest convergence turned out to be $\zeta = 1.66$. The SOR iteration was stopped when the pressure difference between two iteration step was smaller than 10^{-8}.

Because of the staggered grid, only the pressure of the outermost points cannot be calculated by SOR. Therefore, the pressure at the outermost boundary points on the wall surface $p(i, 0)$ were obtained by calculating first the pressure derivative $\partial p/\partial y$ at $p(i, 1)$ with the y-direction Navier–Stokes equation (3), neglecting $\partial v/\partial t$ and $\partial^2 v/\partial x^2$. Then, the pressure $p(i, 0)$ was linearly extrapolated from the pressure $p(i, 1)$ with the calculated pressure derivative. The surface pressure $p_s(i)$ was calculated by equation (9), and the pressure $p(i, J)$ was linearly interpolated from the surface pressure $p_s(i)$ and $p(i, J-1)$. The pressure at the outflow boundary $p(I, j)$ was obtained with the backward difference formula by using the points $p(I-3,j)$, $p(I-2,j)$ and $p(I-1,j)$:

$$p(I,j) = p(I-1,j) + [3p(I-1,j)-4p(I-2,j)+p(I-3,j)]/2. \quad (16)$$

The displacement of the surface was calculated after every time step from the surface velocity by using $\Delta x_s = u_s \Delta t$, $\Delta y_s = v_s \Delta t$ and from the increase of the film thickness due to the condensation.

As for the initial condition, the film thickness $\delta(i)$, the velocities $u(i,j)$ and $u_s(i)$, and the temperature $T(i, j)$ were provided from the Nusselt theory [1]. The velocity $v(i, j)$ was set to zero. The pressure $p(i, j)$ is the same as the surface pressure $p_s(i)$ calculated from equation (9).

Starting from the initial conditions, the calculations were first done to steady state. The steady state is reached when on the one hand the time-averaged velocities and film thickness as well as the root mean square (rms) velocities are not changing any more. On the other hand, when the simulation time is bigger than the traveling time of a particle on the surface from the beginning to the outflow point, results were then taken from calculation sets of a real time of one second.

4. RESULTS

Propagations of the waves on the film surface are shown in Fig. 1. The lines are shown at every 1/16 s. In the abscissa, time-averaged film Reynolds number *Re* is also indicated at some locations. As reported in the previous paper [11] small ripple waves appear at the line of inception and it is not a fixed location. The amplitude of the wave grows rapidly from the small amplitude of ripple waves to the same order of the film substrate and after the strong growth the amplitude increases only slightly.

Figure 2 shows the comparison between the present result and the Nusselt theory in the condensation number *Nu* vs the film Reynolds number *Re* diagram. *Nu* and *Re* of the simulation result are time-averaged values. Experimental data for R11 by Uehara and Kinoshita [8] are also plotted in this figure. In the

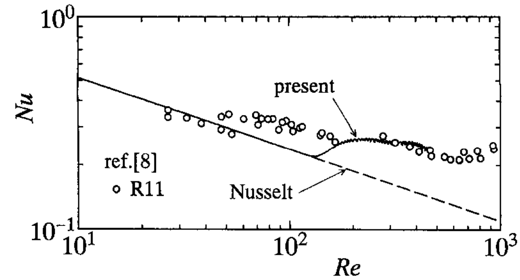

Fig. 2. Time-averaged condensation number of the present simulation and comparison with the Nusselt theory and experiments.

region of $Re < 120$, where the film flow is laminar and the film surface is smooth or has only small ripple waves, *Nu* of the present result has the same value as obtained from the Nusselt theory. At $Re = 120$, *Nu* of the present result becomes bigger than that of the Nusselt theory and the difference increases strongly until $Re = 200$. In the region of $Re > 200$, *Nu* of the present result decreases slightly and agrees well with the experimental data. For the experimental results, *Nu* is bigger than the Nusselt theory in the range $Re > 50$. The earlier increase of the experimental data from the simulation result may be caused by disturbance from the outside of the experimental apparatus. As mentioned before, the line of inception is moving and it will be able to change with an artificial disturbance. The starting point of increasing *Nu* is, therefore, not so important at this stage.

Variation of the heat transfer coefficient in the x-direction is indicated in Fig. 3. In this figure the present result, the Nusselt theory and $k/\bar{\delta}$ are plotted for comparison. $\bar{\delta}$ is the time-averaged film thickness of the simulation results and $k/\bar{\delta}$ represents the heat transfer coefficient of a laminar film with thickness $\bar{\delta}$. In the range of $2000 < x < 4413$, which corresponds to $214 < Re < 455$, the heat transfer coefficient of the present result is about 1.5–1.7 times that of the Nusselt theory. In the same range of x, $k/\bar{\delta}$ is about 1.4–1.6 times that of the Nusselt theory. These facts mean that the heat transfer coefficient is enhanced mainly

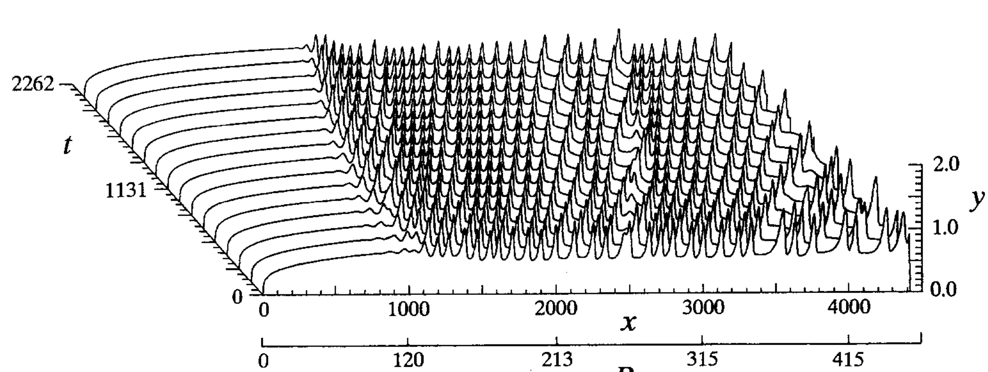

Fig. 1. Instantaneous film shape in the whole calculation region every 1/16 s after the steady state.

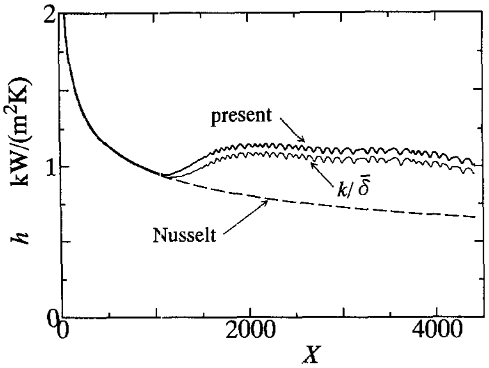

Fig. 3. Variation of time-averaged heat transfer coefficient in the x-direction.

by the decrease of the mean film thickness and the disturbance effects of waves are small.

The instantaneous velocity and temperature fields in two different locations, which are $895 < x < 1175$ and $3190 < x < 3470$, are displayed in Fig. 4a–d. The velocity vectors are shown in Fig. 4a and c, and the contour lines of temperature are shown in Fig. 4b and d. The influence of the waves on the velocity field reaches about $y = 0.5$ for the small ripple wave in Fig. 4a, and about $y = 0.2$ for the big waves in Fig. 4c. As reported in the previous paper [11], although the wave amplitude is already big compared to the substrate thickness, the waves are still not roll waves. In Fig. 4b and d, the peaks of the contour lines near the wall surface are upstream compared with the peaks near the film surface. The location which has the smallest temperature gradient on the plate surface is not the same location of the wave crest which has the thickest film. This means that the effects of the convection on the temperature field cannot be ignored when the wave generated on the film surface even if it is not a roll wave.

Figure 5a–d shows the instantaneous velocity profiles at $x = 3298$, 3339, 3356 and 3402, which correspond to locations at the wave rear, at the wave crest, at the wave front, and at the substrate region, respectively. In these figures, the parabolic velocity profiles with the calculated surface velocity u_s, and the velocity profiles of a laminar falling film flow with the same film thickness, which is calculated from the Nusselt theory and has the surface velocity $(u_s)_N$, are also plotted with dotted lines and chained lines, respectively. The velocity profiles of the present results are approximately similar to the parabolic profiles, while it is slightly different at the wave crest. The velocities of the present results are smaller than those of the Nusselt theory at the wave crest and the wave front, and bigger at the wave rear. At the substrate region, the present result has approximately the same velocity as the Nusselt theory.

Figure 6a–d shows the instantaneous temperature distributions at the same locations as Fig 5a–d. The linear temperature distributions are also plotted with dotted lines. The temperature distributions are convex

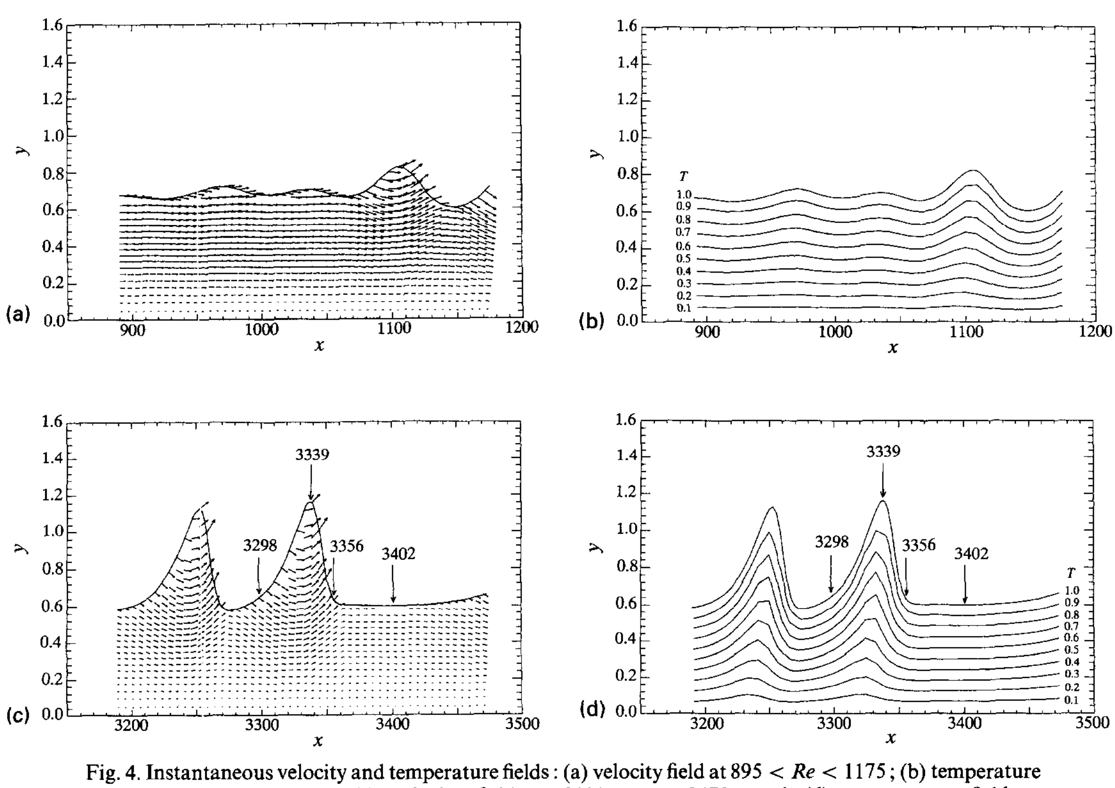

Fig. 4. Instantaneous velocity and temperature fields: (a) velocity field at $895 < Re < 1175$; (b) temperature field at $895 < Re < 1175$; (c) velocity field at $3190 < Re < 3470$; and (d) temperature field at $3190 < Re < 3470$.

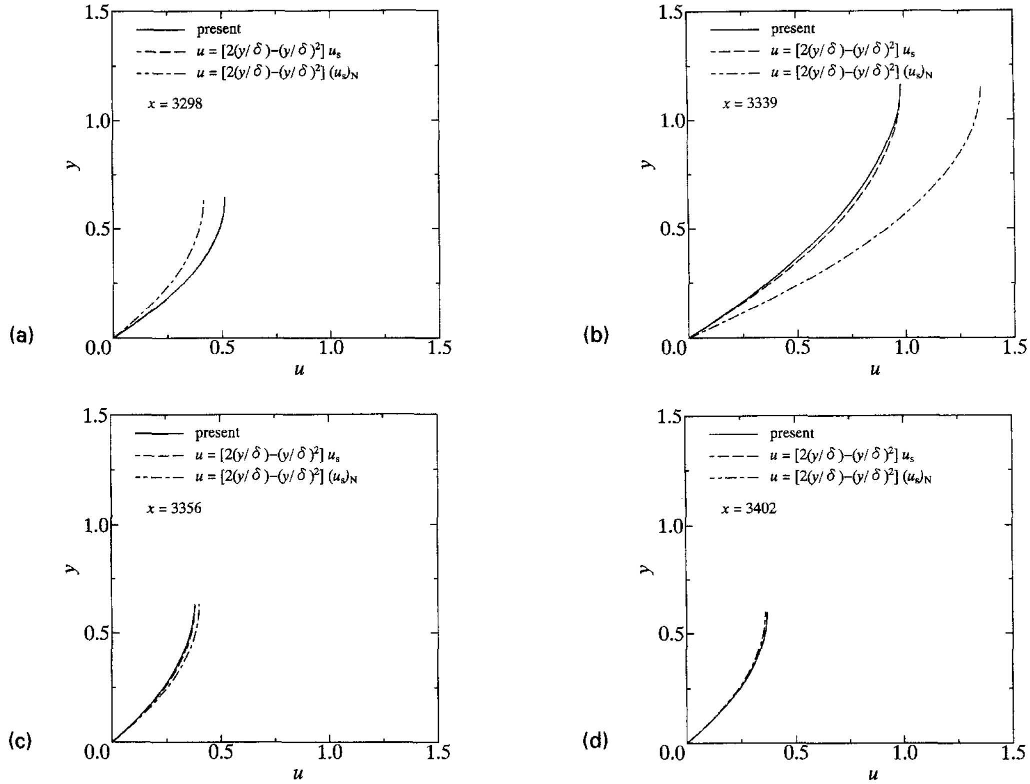

Fig. 5. Instantaneous velocity profiles: (a) at wave rear $x = 3298$; (b) at wave crest $x = 3339$; (c) at wave front $x = 3356$; and (d) at substrate region $x = 3402$.

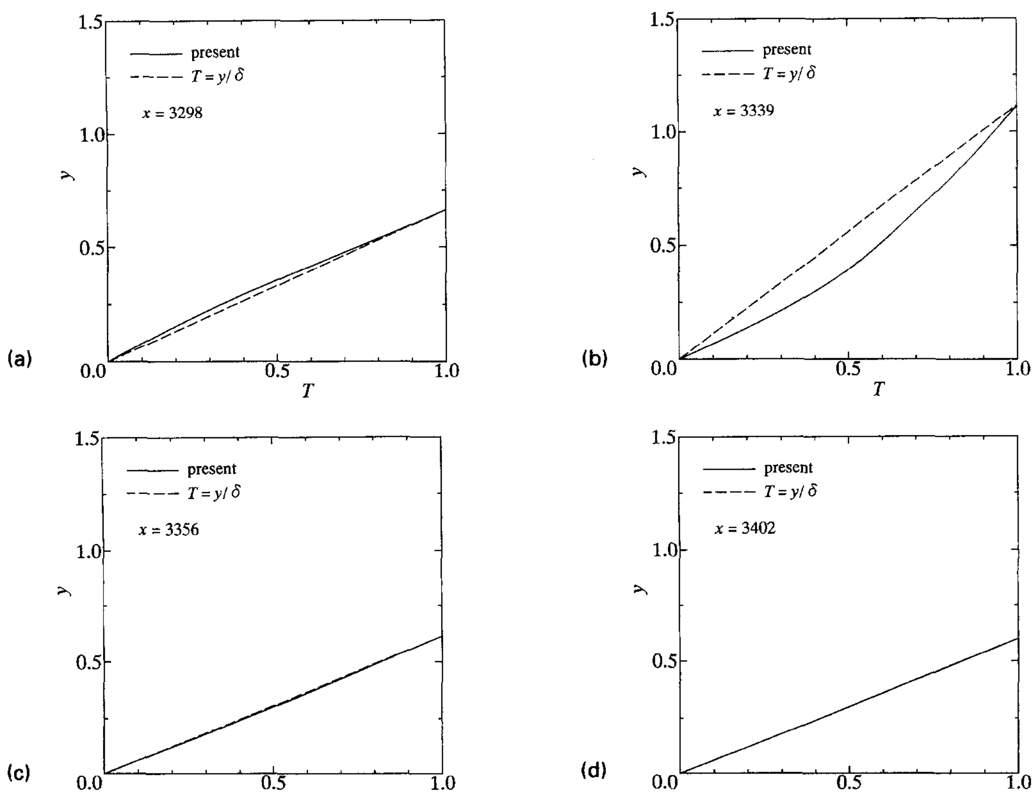

Fig. 6. Instantaneous temperature distributions: (a) at wave rear $x = 3298$; (b) at wave crest $x = 3339$; (c) at wave front $x = 3356$; and (d) at substrate region $x = 3402$.

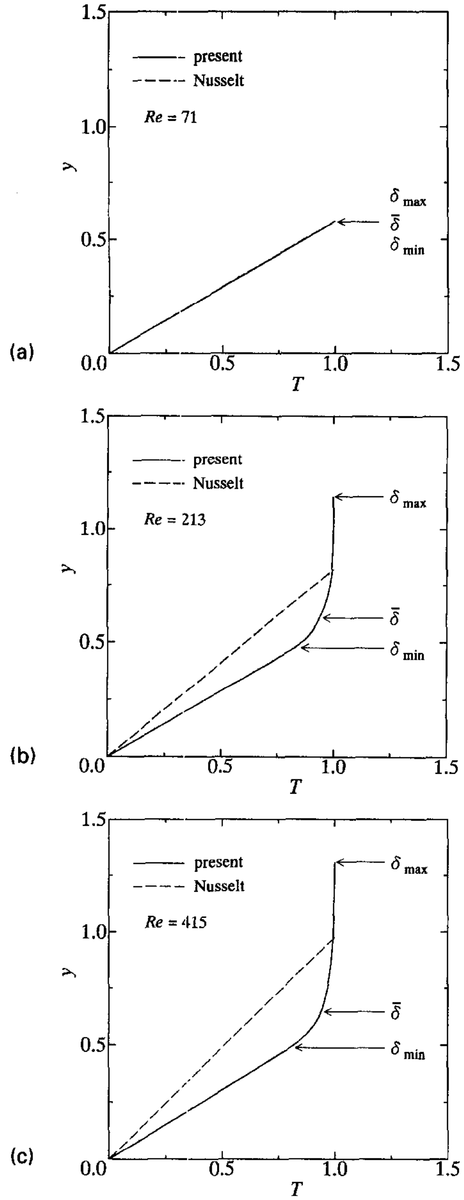

Fig. 7. Time-averaged temperature distributions: (a) at $Re = 71$; (b) at $Re = 213$; and (c) at $Re = 415$.

at the wave rear, $x = 3298$, and concave at the wave crest, $x = 3339$, and are almost linear at the wave front, $x = 3356$, and at the substrate region, $x = 3402$. At the wave crest, the temperature gradient at the wall surface is bigger than that of the linear distribution. Although the instantaneous velocity profiles are approximately parabolic, such as laminar flow, the temperature distributions are affected by convection effects.

Figure 7a–c shows time-averaged temperature distributions for $Re = 71, 213$ and 415, which correspond to the dimensionless distances at $x = 494$, 1994 and 3982. Temperature distributions calculated from the Nusselt theory are also plotted for the identical Reynolds numbers. The locations of the time-averaged film thickness $\bar{\delta}$, the maximum and minimum film thicknesses δ_{max} and δ_{min} are indicated with arrows. For $Re = 71$, the present result is identical to the Nusselt theory. For $Re = 213$ and 415, the calculated results have linear distributions below the minimum film thickness, and have a bigger temperature gradient at the wall surface than for Nusselt theory.

5. CONCLUSIONS

A falling condensate film with waves on the vapor–liquid interface has been analyzed with the direct computer simulation. The simulation is conducted for a condensate film of R11 on a vertical wall from the leading edge to 0.6 m and the film Reynolds number reached 455. Waves which have an amplitude of the order of the film substrate have been observed at $200 < Re < 455$, however, they are still not roll waves. The Nusselt number of the calculated results agrees well with experimental data in the wavy region at $200 < Re < 455$, and with the Nusselt theory in the laminar region at $Re < 120$. Although the instantaneous velocity profiles are approximately parabolic, such as laminar flow, the instantaneous temperature distributions are affected by the convection effects. On the other hand, the time-averaged temperature distributions are, however, almost linear within the minimum film thickness, where liquid is always in existence. The enhancement of the heat transfer coefficient is attributed mainly to the decreasing of the time-averaged film thickness due to the waves and the disturbance effects of waves are small. Since the computational mesh is too big to capture the small turbulence motion and the film Reynolds number is small, the turbulence level in the substrate and the influence of the turbulence on the heat transfer coefficient cannot be indicated, but remain for future investigations.

REFERENCES

1. W. Nusselt, Die Oberflaechenkondensateion des Wasserdampfes, *VDI Zeitschrift* **60,** 541–546, 569–575 (1916).
2. F. L. Shea and N. W. Krase, Drop-wise and film condensation of steam, *Trans. AIChE. J.* **36,** 463–487 (1940).
3. G. V. Ratiani and I. G. Shekriladze, An experimental study of the heat exchange process on transition from laminar to turbulent flow of the film, *Thermal Engng* **11,** 101–103 (1964).
4. R. Gregorig, J. Kern and K. Turek, Improved correlation of film condensation data based on a more rigorous application of similarity parameters, *Wärme- Stoffübertrag.* **7**, 1–13 (1974).
5. G. Selin, Heat transfer by condensing pure vapors outside inclined tubes, *International Development in Heat Transfer, Proc. Heat Transfer Conf.* (Part II), University of Colorado, Boulder, CO, pp. 279–289 (1961).
6. H. Struve, Heat transfer to an evaporating falling refrigerant film, *12th Congr. International Institute of Refrigeration*, Madrid (1967).
7. K. R. Chun and R. A. Seban, Heat transfer in evaporating liquid films, *J. Heat Transfer* **93,** 391–396 (1971).
8. H. Uehara and E. Kinoshita, Wave and turbulent film

condensation on a vertical surface (correlation for local heat transfer coefficient), *Trans. JSME* **60-577**, 3109–3116 (1994) (in Japanese).
9. R. I. Hirshburg and L. W. Florschuetz, Laminar wavy-film flow: Part I, hydrodynamic analysis, *Trans. ASME J. Heat Transfer* **104,** 452–458 (1982).
10. R. I. Hirshburg and L. W Florschuetz, Laminar wavy-film flow: Part II, condensation and evaporation, *Trans. ASME J. Heat Transfer* **104,** 459–464 (1982).
11. E. Stuhlträger, Y. Naridomi, A. Miyara and H. Uehara, Flow dynamics and heat transfer of a condensate film on a vertical wall—I. Numerical analysis and flow dynamics, *Int. J. Heat Mass Transfer* **36,** 1677–1686 (1993).
12. T. Kawamura and K. Kuwahara, Computation of high Reynolds number flow around a circular cylinder with surface roughness, A.I.A.A. Paper No. 84-0340, pp. 1–11 (1984).
13. M. A. Shapiro and J. J. O'Brien, Boundary conditions for fine-mesh limited-area forecasts, *J. Appl. Meteorol.* **9,** 345–349 (1970).
14. P. L. Kapitza and S. P. Kapitza, Wavy flow of thin layers of viscous fluid, *Collected Papers of P. L. Kapitza*, Vol. 2, pp. 662–709. Pergamon Press, New York (1965).
15. K. J. Chu and A. E. Dukler, Statistical characteristics of thin wavy films, Part II. Studies of the substrate and its wave structure, *AIChE J.* **20,** 695–706 (1975).